BOREAL ENVIRONMENT RESEARCH 16 (suppl. A): 84–102
ISSN 1239-6095 (print) ISSN 1797-2469 (online)

Helsinki 31 March 2011

Circulation patterns in the Gulf of Finland derived from the EOF analysis of model results

Jüri Elken, Marden Nõmm and Priidik Lagemaa

Marine Systems Institute at Tallinn University of Technology, Akadeemia tee 21, EE-12618 Tallinn, Estonia

Received 7 Dec. 2009, accepted 27 Aug. 2010 (Editor in charge of this article: Kai Myrberg)

Elken, J., Nõmm, M. & Lagemaa, P. 2011: Circulation patterns in the Gulf of Finland derived from the EOF analysis of model results. *Boreal Env. Res.* 16 (suppl. A): 84–102.

For the Gulf of Finland, we carried out the EOF (empirical orthogonal functions) analysis of hourly forecasts from the Baltic Sea operational HIROMB-SMHI model for the period 2006–2008. It is possible to distinguish two regions with a specific regime of circulation variability. The western region behaves like a wide channel. Dominant EOF modes at different sections have similar patterns and their time-dependent amplitudes are well correlated. A prevailing mode of currents (23%–42% of the variance) is barotropic (unidirectional over the whole section) and its oscillation (spectral peak at 24 h) is related to the water storage variation of the Gulf. A two-layer flow pattern (surface Ekman transport with deeper compensation flow, 19%–22%) reveals both inertial and lower frequencies. Highest outflow of surface waters occurs during north-easterly winds. The eastern wider region has more complex flow dynamics and only patterns that are nearly uniform over the whole Gulf were detected here. On the sea surface, quasi-uniform drift currents are deflected on the average by 40° to the right from the wind direction and they cover 60% of the circulation variance. Sea level variability is heavily (98%) dominated by nearly uniform changes which are caused by the water storage variations of the Gulf. Sea level gradients contain the main axis (23%) and transverse (17%) components, forced by winds of the same direction. The flows below the surface are decomposed also into the main axis (24%–40%) and transverse (13%–16%) components that are correlated with the sea level gradients according to the geostrophic relations.

Introduction

Large estuarine basins exhibit general cyclonic circulation in the northern hemisphere. Along-basin density gradients, created by the freshwater discharge at the head and deeper inflow of more saline waters on the ocean boundary, are modified by the transverse flows and diapycnal mixing (Chant *et al*. 2007). However, the circulation is highly variable due to the wide range of involved processes. Variable circulation patterns of the marginal seas are not so well established as compared with the atmospheric circulation patterns.

The Baltic Sea is a multi-basin estuarine sea with multidude scales of oceanographic variability. The mean surface circulation in the subbasins is cyclonic (Palmén 1930). On the shorter time scales (less than a few months) currents and stratification are modified by the variable forcing, such as moving weather patterns and fluctuat-

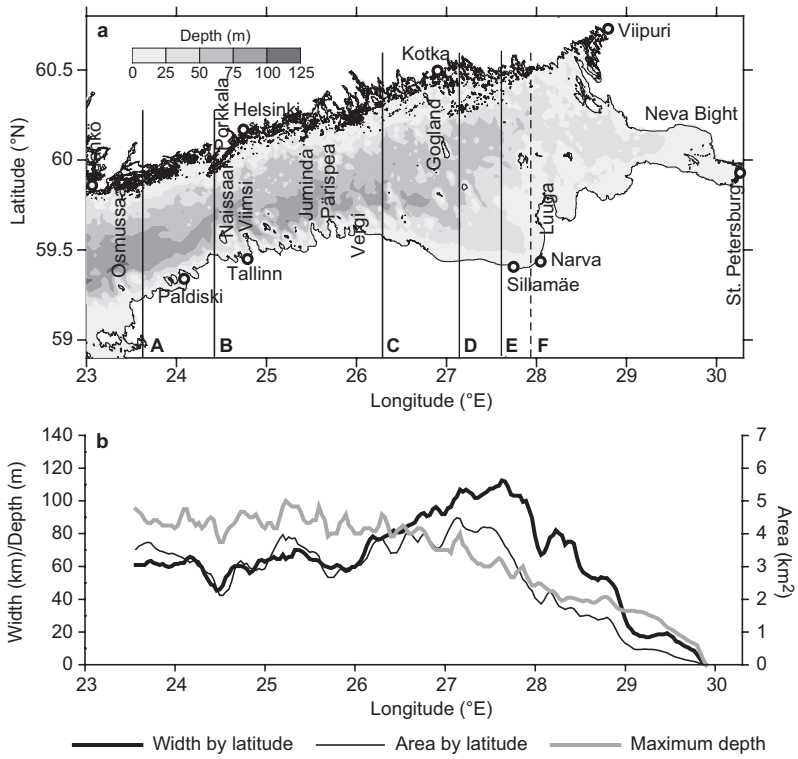

Fig. 1. Topography of the Gulf of Finland: (**a**) a map with depth contours, (**b**) longitudinal distributions of transverse width and area of the offshore regions with depth more than 10 m, and maximum depth. Letters A to E denote the sections for cross-channel analysis, A to F is the region of horizontal pattern analysis.

ing water exchange on the outer boundary of the basin (Matthäus and Schinke 1999). Unsteady circulation components may include propagation of long gravity waves of tidal and/or storm surge origin (Jönsson *et al*. 2008), Ekman transport of the upper layer and compensating deeper flows (Krauss and Brügge 1991), their evolution into upwelling/downwelling patterns (Lehmann and Myrberg 2008) and/or quasi-steady wind circulation patterns characteristic to the lakes and channels without lateral density gradients. Adjustment to the changed forcing is governed by the generation and decay of inertial waves (Nerheim 2004) and barotropic/baroclinic Kelvin waves (Lass and Talpsepp 1993). There is also a mesoscale component not always directly related to the forcing fields, comprised mainly of mesoscale fronts and eddies (Reissmann *et al*. 2009).

The Gulf of Finland is an elongated estuarine basin of the Baltic Sea (Fig. 1a), located east from the Hankö–Osmussaar line, that has the highest specific freshwater discharge (per unit area and unit volume of the basin) among other Baltic Sea sub-basins (e.g. Bergström and Carlsson 1994). With the reference to the estuarine terminology, the head is located in the east where the Neva River, entering through St. Petersburg, discharges 2400 $m^3 s^{-1}$ of freshwater (66% of the Gulf of Finland runoff), the largest amount among Baltic rivers. In the west, there is a free connection of the Gulf to the Baltic Proper without a topographical constriction and/or sill. Overall length of the Gulf from west to east is about 400 km. Despite the channel-like general shape, the width of the Gulf is quite variable. The western part, extending from the entrance at about 23.5°E to 26°E near the Vergi Peninsula, has quite uniform meridional width (Fig. 1b) of about 60–70 km, counted by depths greater than 10 m. Maximum depth by latitude is from 80 to 100 m. In this part, the Gulf has contractions near 24.5°E–24.8°E (from Naissaar and Viimsi to Porkkala) and 25.6°E–25.9°E (near the Juminda and Pärispea Peninsulas), where the width decreases by 20%–30% and the cross-section area by 40%–50%. East from 26°E, the central basin widens up to 110 km (excluding the shallow areas) at 27.6°E near Sillamäe. Maximum depth decreases to 60 m. Further to the east from Narva towards the Neva Bight, the Gulf

gets more narrow and shallow.

Salinity and density fields in the Gulf of Finland exhibit some features of a partially mixed estuary. The mean horizontal circulation is cyclonic — with average inflow of the more saline water close to the southern, Estonian coast and outflow of the less saline water along the northern, Finnish coast. Speeds of the mean circulation have been estimated a few cm s^{-1}. However, the circulation is modified by several factors, as described above. Instantaneous currents may reach 20–30 cm s^{-1} or even more (Alenius *et al*. 1998).

Over the seasons, changes of stratification and wind forcing create different mean patterns of circulation in the Gulf of Finland, as described already by Witting (1912) and Palmén (1930) (*see* the review by Alenius *at al*. 1998). Instrumental observations give reliable estimates of the variability of currents, but unfortunately they are limited either in time or space to give estimates of the current patterns and their variations. Therefore, the present circulation estimates are based, to a large extent, on the model results.

Multiannual model studies (Lehmann *et al*. 2002, Andrejev *et al*. 2004, Meier 2005) have reconfirmed the observational arguments of the mean cyclonic circulation. The results gave further insight into the problem of persistency of the current direction, i.e. fraction of the vector-mean current speed to the scalar-mean speed (Palmén 1930). Within the limits of model performance, the earlier observation-based indications were renewed by the concepts of high-stability current belts, where persistency above 0.5 (Andrejev *et al*. 2004) is concentrated in the outflow region, to the north from the central axis of the Gulf.

The present paper is aimed to study the unsteady circulation patterns of the Gulf of Finland, using the available hourly model results from the operational HIROMB-SMHI model system for the period 2006–2008. Using the empirical orthogonal functions (EOF) method, we decompose the large-scale circulation variability into dominating, objectively determined patterns/modes of the temporally variable amplitude. When possible, we draw out the relations of the EOF amplitude variations to the variations in external forcing. This way we contribute to the existing circulation knowledge both in the statistical and physical (oceanographic) sense.

Material and methods

Model data

We used the results from the operational HIROMB-SMHI model system (Funkquist 2001, Gästgifvars *et al*. 2008) for the period 2006–2008. The model domain covers the whole Baltic Sea and its extension to the North Sea (9.375°E–30.236°E, 53.658°N–65.892°N) with a grid step 5/3´E by 1´N (about 1 nautical mile) yielding 752 × 735 horizontal grid points. The model presents the Baltic Sea by 16 vertical layers, with a grid step of 4 m from the surface down to 12 m, 6 m further down to 30 m, 10 m down to 60 m and increasing further below. The model has mixing modules based on the κ-ω approach (Umlauf *et al*. 2003) for vertical mixing and Smagorinski formulation for horizontal mixing. It has also an extensive ice mechanics and thermodynamics module. The model is forced by the atmospheric forecasts from the HIRLAM-SMHI model system, with a grid step of 22 km, and river forecasts from the HBV surface water modeling system. Lateral open sea conditions are derived from larger domain models using the nesting technique. Tidal forcing is introduced along the North Sea outer boundary of the largest three-dimensional domain (grid step 12 nautical miles). The system performs data assimilation, based on the different data: remote sensing data of sea surface temperature and sea ice, *in situ* observations at MARNET buoys and from ships, including vertical profiles from the HELCOM stations and daily FerryBox surface section (Tallinn–Helsinki, Lips *et al*. 2008b) data for salinity and temperature.

We have assembled the daily forecasts from two upgrades of the model into one time series. Version 3.0 had been running since 15 Nov. 2005. The next version 3.1 (Axell 2006) started on 19 Sep. 2007. It introduced the variable wind stress coefficient and included effects of the surface waves. Specific to the present study, the sea

surface wind stress components τ_λ, τ_φ along the longitude λ and latitude φ are calculated with a common quadratic formula from the corresponding wind speed components W_λ and W_φ at the height of 10 m as

$$\tau_\lambda = \rho_a c_D W_\lambda \sqrt{W_\lambda^2 + W_\varphi^2} \text{ and}$$

$$\tau_\varphi = \rho_a c_D W_\varphi \sqrt{W_\lambda^2 + W_\varphi^2},$$

where ρ_a is the air density. Until 18 Sep. 2007, the drag coefficient c_D was defined as

$$c_D = 10^{-3}(0.7 + aW)$$

where $W = \sqrt{W_\lambda^2 + W_\varphi^2}$, and $a = 0.09$ (m s^{-1})$^{-1}$.

In order to correct the modeled too high surface current velocities during stronger winds and too low velocities during weaker winds as compared to the observations, the dependence on neutral-stability winds W_N was introduced in version 3.1, $c_D = 1.3 \times 10^{-3}$ at $W_N < 8$ m s^{-1} and $c_D = 10^{-3}(0.84 + a_N W_N)$, $a_N = 0.058$ (m s^{-1})$^{-1}$. Depending on the atmospheric stability (difference of temperature of air and water), the drag coefficient varies at wind speeds below 10 m s^{-1} from 0.9×10^{-3} (most stable) to 1.95×10^{-3} (most unstable).

Recent validation study of six three-dimensional models against more than 300 vertical profiles of temperature and salinity measured in the Gulf of Finland (Myrberg *et al*. 2010) concluded that the best model was HIROMB, although no model was the best/worst in all cases. Another study (Elken *et al*. 2008) showed that on the average, during the warm season HIROMB produces too high surface salinity gradients and too low vertical stratification as compared with the observational data. Sea level validation (Gästgifvars *et al*. 2008, Elken *et al*. 2008) revealed that root mean square errors of 1–24 h sea level forecasts at different coastal stations of the Gulf of Finland are 5–10 cm. Unfortunately, model comparisons with current observations are quite rare. Gästgifvars *et al*. (2006) concluded that during the rapidly changing weather conditions drift trajectories, calculated using the HIROMB-based system Seatrack Web, followed well the observed drifter trajectories in the central part of the Gulf of Finland.

Application of the EOF method

We shall analyze the circulation patterns on the basis of hourly data from the operational HIROMB model system for the period 2006–2008: altogether 25 968 sets of grid data. Within the statistical procedures, we consider the deviations of currents, density, sea level and wind from the 3-year mean fields. The deviation fields are decomposed into spatial modes (fixed over the time period) with time-dependent amplitudes, using the well-known EOF method (e.g. von Storch and Zwiers 1999), which is a Principal Component Analysis. This technique allows for estimating the variance ("energy") contribution of individual spatial modes to the overall variability. The time-dependent amplitudes show, how in specific events different spatial patterns are amplified or damped.

The EOF method is particularly useful when variability of studied fields is *a priori* known to be governed by standing patterns. In the complex range of ocean variability, such cases occur, for example in basin-wide horizontal patterns (Schrum *et al*. 2006), and vertical profiles or sections dominated by low-frequency waves (Lass and Talpsepp 1993, Pizzaro and Shaffer 1998) or flows in a channel (Thomson *et al*. 2007).

For the specific application, let us analyze the set of spatio-temporal data $\psi(i,j,k,n)$, where i, j and k are the indices of space coordinates and n is the time step index. The EOF method is based on the analysis of one-dimensional sets of variables. For this purpose we transform the multi-dimensional data set of the size M at each time step n into a one-dimensional array of index $m = m(i,j,k)$, where m is the data counter in the multi-dimensional data sequencing loop. The reverse transformations of coordinates are $i = i(m)$, $j = j(m)$, $k = k(m)$, which perform remapping of the found EOF features back to the original space. If the time-averaged mean is

$$\overline{\psi(m)}^n = \frac{1}{N}\sum_{n=1}^{N} \psi(m,n)$$

then the fluctuation is

$$\psi'(m,n) = \psi(m,n) - \overline{\psi(m)}^n .$$

The fluctuations can be presented by a superposition

$$\psi'(m,n) = \sum_{l=1}^{L} A_l(n) F_l(m)$$

where the number of modes L equals the number of spatial data points M. Here $F_l(m)$ is a normalized orthogonal spatial structure function (mode) and $A_l(n)$ is the time-dependent amplitude of the mode l. The modes $F_l(m)$ are found as eigenvectors of the (spatial) covariance matrix of $\psi'(m,n)$. Different modes p, q are orthogonal in terms of condition

$$\sum_{m=1}^{M} F_p(m) F_q(m) = 0 \text{ if } p \neq q.$$

Then the amplitudes of EOF modes are found in the form

$$A_l(n) = \sum_{m=1}^{M} \psi'(m,n) F_l(m).$$

The variance (energy) contained in a particular mode l is determined as the ratio of the corresponding eigenvalue λ_l to the sum of all eigenvalues over L. The modes are usually numbered by the decreasing variance, with the 1st mode containing the largest fraction of the overall variance. Note, that the analyzed dataset $\psi(m,n)$ may also contain components of physical vectors such as currents and winds.

Analysis of EOF mode patterns and amplitudes

Classical EOF method uses normalized non-dimensional modes

$$\sum_{m=1}^{M} F_l^2(m) = 1$$

and dimensional amplitudes $A_l(n)$. However, the interpretation of the numerical results of such a presentation depends on the number of selected spatial data points M. As an alternative (e.g. von Storch and Zwiers 1999), we use the dimensional spatial modes

$$\sum_{m=1}^{M} \tilde{F}_l^2(m) = \lambda_l$$

and the non-dimensional amplitudes $\tilde{A}_l(n)$ scaled to yield their standard deviation equal to 1. Therefore, if we consider $\tilde{A}_l(n) = 1$ as a typical event then graph of the individual mode $\tilde{F}_l(m)$ presents the physical values of the spatial pattern of this event.

We chose to study the EOF modes at selected fixed levels (horizontal patterns) and in selected meridional (nearly cross-gulf, deflection angle up to 15°) sections. Although we also performed some analysis of the monthly and tri-monthly data sub-sets over 3 years, the final selection was one data set over the whole period since the mode patterns turned out to be quite similar. Transects (Fig. 1) were selected along longitudes 23.65°E (section A), 24.38°E (B), 26.26°E (C), 27.13°E (D) and 27.60°E (E). The area for the horizontal pattern analysis was confined between 23.65°E (A) and 27.93°E (F). Sections contained up to 250 active grid points (section B) and horizontal patterns up to 3714 points (surface analysis).

We seek the physical interpretation of the formal EOF patterns and their relation to forcing by analyzing the time series of EOF amplitudes of different modes, using correlation analysis and power spectra analysis. The overall length of hourly amplitudes was 25 968 points. Due to this large sample size, correlations were statistically highly significant even for low correlation values. However, for oceanographic reasons (low-frequency events may be quite rare within a few years) we did not consider the relations, whose coefficients of determination (R^2) were below 0.4. Spectral analysis was done using the Welch averaged periodogram method built in the MATLAB. The data was divided into about 100 overlapping segments by setting the Hamming filter window length equal to 512, with the overlap length equal to 256 (50% of the window). Power spectral densities were calculated then as the average of the periodograms of individual segments.

The vector fields, like winds and currents over a horizontal area, were analyzed by mapping the vector components at different grid points into the one-dimensional array and remapping the derived modes $\tilde{F}_l(m)$ back to the original vector components and grid points. Many of the vector patterns appeared to be quite non-divergent. For the visualization of vectors, we used the streamfunction approach (Watterson 2001) if R^2 for the correlations between the origi-

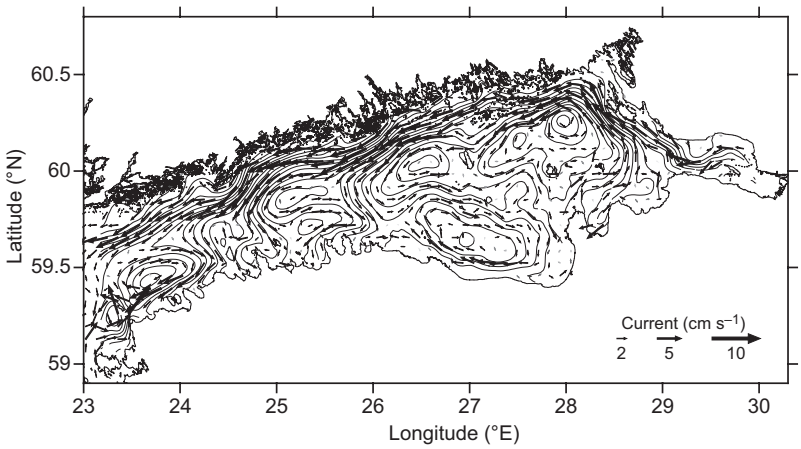

Fig. 2. Mean circulation of period 2006–2008 in the most stable layer (4–8 m) of the Gulf of Finland. The currents are presented by every 4th vector superimposed by the streamfunction contours.

nal vectors and the vectors calculated from the streamfunction exceeded 0.6.

Mean circulation

The period 2006–2008 was characterized by mild to moderate winters and normal wind regime. The mean wind vector, based on the forcing data in the central part of the Gulf, was about 2 m s^{-1} from 240°–250° as within the longer period. However, several significant meteorological and oceanographic events occurred. Intensive upwelling occurred along the southern coast in July–August 2006 (Lips *et al*. 2008a), due to the unusually persistent easterly winds. Stormy periods in October–November 2006 and in January 2007 caused high sea levels in the Gulf due to the southwesterly winds (Elken *et al*. 2008).

The mean current fields (Fig. 2) reveal the known cyclonic circulation. The currents in the most stable layer of 4–8 m, just below the drift-influenced surface layer, reveal the maximum outflow of less saline water near the Finnish coast in the Finnish Coastal Current (Stipa 2004). As compared with the earlier results, Andrejev *et al*. (2004) — who used the OAAS model — obtained the mean outflow in 1987–1992 closer to the main axis of the Gulf. The shift can be explained by the differences of the specific forcing events during different periods (although the mean wind vectors were the same), and the specific features in the response of the two models under the same forcing (Myrberg *et al*. 2010). Both the HIROMB-SMHI model (present study) and the OAAS model (Andrejev *et al*. 2004) reveal some other interesting circulation features. The southward recirculation loop, detaching from the Finnish Coastal Current and feeding the southern eastward currents, is located just east from the Tallinn–Helsinki connection line. We also note the second southward loop of the Finnish Coastal Current near 26°E (Fig. 2). In the eastern part of the Gulf, from 26.5°E to 27.7°E, the currents near the southern coast are oriented in reverse, westward direction. An unexplained circulation feature appears in the western part of the southern coast, west from 24.4°E (Fig. 2). Namely, the coastal currents are directed westwards and the inflow of more saline open Baltic Sea waters takes place offshore, in the deepest parts of the Gulf.

Vertical structure of the mean currents in section B (Fig. 3) exhibits the outflow on the northern slopes of the Gulf, some 10–15 km offshore, at the depths of 10–20 m. Inflow takes place in the deepest part of the Gulf in two depth ranges, close to the surface and in the halocline within the depths from 40 to 60 m. The mean sea level drops by 2–3 cm from north to south, forcing the outflow of surface waters in accordance with the geostrophic relations. Towards greater depths, the density gradients oppose the sea level drop, resulting in the decrease of pressure gradients and along-channel flow.

Note that all the further pattern variation analysis is based on the deviations (anomalies) from the mean fields given in this section.

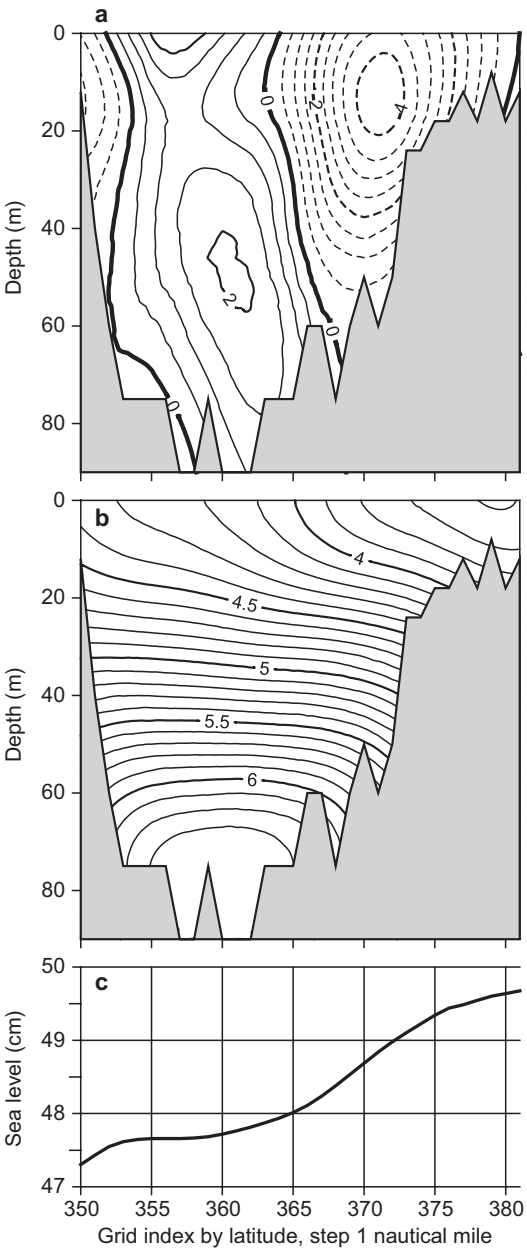

Fig. 3. Mean (**a**) east-west currents, (**b**) density , and (**c**) sea level in section B of the period 2006–2008. The contours for currents and density anomalies are cm s^{-1} and kg m^{-3}, respectively.

EOF modes of circulation variables

Horizontal fixed level modes

We started the analysis of horizontal modes in a region from A to F (the wide part of the Gulf, Fig. 1b) from wind vectors, considering as usual deviations from the mean fields. The two first wind vector modes comprise 93% of the wind field variance. Horizontally the modes are almost uniform: the relative standard deviation of vector magnitudes is only 3%; therefore, we may also calculate standard deviation of directions and conclude that it is less than 2° (for the small relative vector magnitudes the direction is quite uncertain, but this is not the case here). It means that on the average "physical" wind vectors of the two first EOF modes are geometrically almost orthogonal (perpendicular) at each horizontal grid point. Note, that individual modes are exactly orthogonal in terms of EOF eigenvector scalar product over the whole domain, not necessarily the "physical" vectors at each grid point. Within this analysis, 53% of the wind variance (1st mode) is oriented along direction 226° (SW–NE) or 46° (according to the EOF sign determination options) and 40% (2nd mode) along 316° (NW–SE) or 136°. This result justifies common usage of the horizontally uniform, only time-dependent wind field in modeling studies of sub-regions, which extent is much smaller than baroclinic Rossby radius of the atmosphere (about 1000 km, Gill 1982).

Wind-driven surface currents are generally known to follow the wind stress, but they are deflected from the wind direction due to the Earth's rotation. The two first current modes (deviations from the mean fields, Fig. 4) comprise together 60% of the variance. They also exhibit horizontally quasi-uniform patterns like the wind modes, but the spatial variability of the vector magnitudes is somewhat higher. Still, the directional variation study is justified and the standard deviation is 18°–20°. Main variations of the surface current direction take place in the coastal areas and between the western and eastern parts of the calculation area. Within the sign determination freedom of EOF modes, the mean direction is 104° or 284° for the 1st mode and 16° or 196° for the 2nd mode. It means that on the average the 1st and 2nd surface current modes are geometrically perpendicular within ±2° accuracy. As shown in Fig. 4, the 3rd and 4th modes of surface currents do not comprise horizontally uniform drift patterns. Instead, they

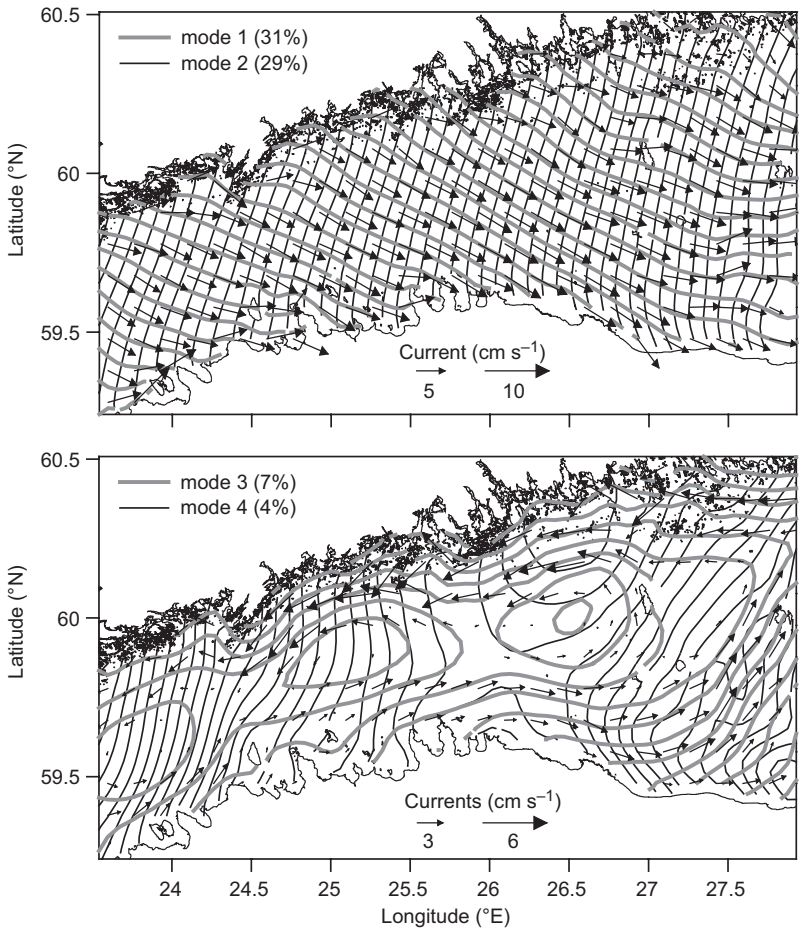

Fig. 4. Horizontal EOF mode patterns of surface current, 1st and 2nd mode (top panel), 3rd and 4th mode (bottom panel). The vector patterns of modes are visualized by the streamfunction method. For comparison, actual vectors of the 1st and 3rd mode are also drawn.

reveal a number of circulation cells where the mean direction does not make sense. A characteristic feature of the 3rd mode (7% of variance) is opposite currents along the southern and northern coasts of the channel, and partial circulation closures at longitudes 24.5°E–24.8°E and 25.6°E–25.9°E, where the cross-channel geometry shows contractions.

Further, we studied how the amplitudes of the two first modes of surface currents A_{u1} and A_{u2} are related to the amplitudes of wind modes A_{W1} and A_{W2}. Since the surface currents have notable energy near the inertial period of 14 h as obtained from the spectral analysis of A_{u1} and A_{u2}, we used for their suppression a 3-point filter:

$$\tilde{\psi}(t) = 0.25\left[\psi(t - T/2) + 2\psi(t) + \psi(t + T/2)\right]$$

(here ψ and $\tilde{\psi}$ are original and filtered variables, T is the period to be damped). We found that amplitudes A_{u1} and A_{u2} of the two first current modes correlate well with the wind stress functions $A_{W1}\sqrt{A_{W1}^2 + A_{W2}^2}$ and $A_{W2}\sqrt{A_{W1}^2 + A_{W2}^2}$ of the amplitudes of the two first wind modes A_{W1} and A_{W2}, if the physical vectors of wind stress amplitudes are projected to a proper angle. The best correlations (R^2 = 0.71) with both A_{u1} and A_{u2} were obtained when wind amplitudes A_{W1} and A_{W2} were rotated as horizontal vector components (with respect to EOF mode directions 46° and 136°, respectively) clockwise by 20°. This means that current component A_{u1} towards 104° correlates with the wind stress towards 66° (i.e. 46° + 20°) and component A_{u2} towards 196° correlates with the wind stress towards 156° (136° + 20°). From the above we conclude that 60% of the surface current variance is explained by the relation: speed of the surface currents is proportional to the wind stress (wind speed squared) and the currents are deflected

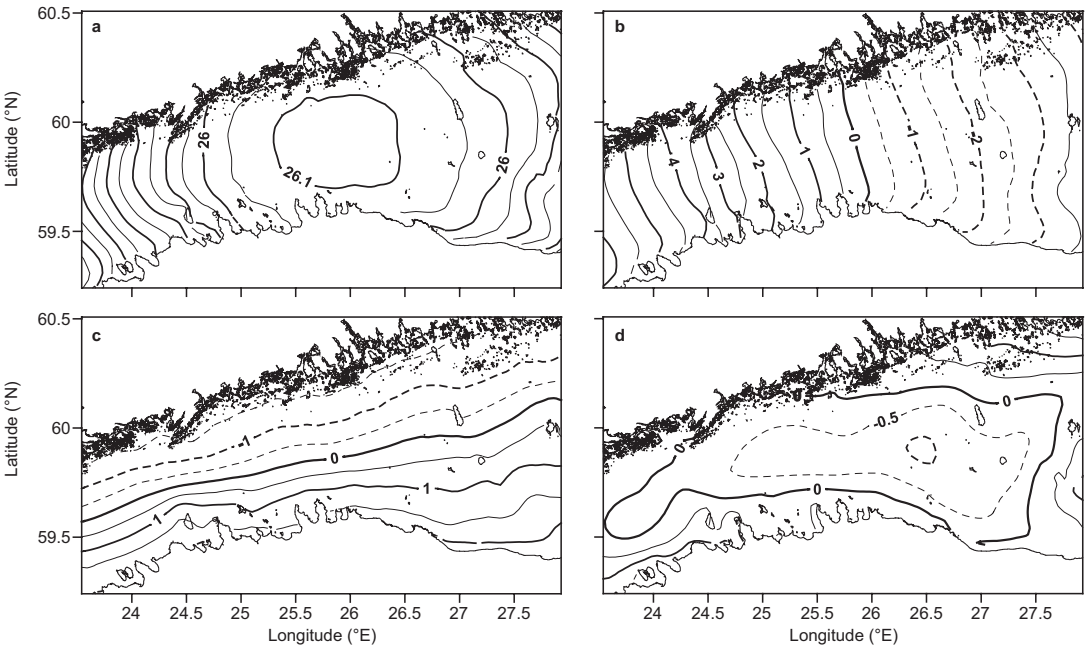

Fig. 5. Horizontal EOF mode patterns of the sea level, modes: (**a**) mode 1 (98.6%), CI = 0.05 cm; (**b**) mode 2 (1.0%), CI = 0.5 cm; (**c**) mode 3 (0.2%), CI = 0.5 cm; and (**d**) mode 4 (0.03%), CI = 0.5 cm;. The mode patterns are dimensional (cm), scaled by the square root of the variance of each mode. Note the smaller contour interval for the flat 1st mode.

on the average 40° to the right from the wind direction. Although several observational studies revealed linear dependence between the wind speed and the surface current speed (*see* the review by Alenius *at al*. 1998), we found in case of prevailing EOF modes a better correlation match between current speed and quadratic wind stress. It is interesting to note that scatter plots of amplitudes of wind stress functions and surface currents revealed two distinct clusters during the whole period 2006–2008. These clusters correspond to the older model version 3.0 with linear drag coefficient dependence on the wind speed, and to the new version 3.1 with stability-dependent wind stress drag coefficient. The values of R^2 were 0.84–0.86 for the old version and 0.77 for the new version. From old to new version, the wind-to-current transfer coefficient decreased by about 2 times. We note that these relation changes reflect only the revision of model features, not the circulation physics. The 40° deflection angle of the current anomalies (from the mean fields) relative to the wind anomalies is the same for both model versions. From the earlier studies, based on observations at specific locations, the deflection angle (including the mean fields) could be up to 60° (Gästgifvars *et al*. 2006).

Sea level variability is heavily (98.6% of variance) dominated by the flat 1st mode, where difference of the minimal and maximal values is only 2% of the mean value of the mode (Fig. 5). This mode thus presents storage variations (filling and emptying) of the whole gulf, with negligible spatial gradients. Quite expectedly, the amplitudes of this mode are not correlated with the local wind amplitudes, since the storage variations of the particular gulf depend on the mean sea level of the whole Baltic Sea and the large-scale air pressure and wind fields over the whole sea area (Lehmann and Hinrichsen 2001, Lehmann *et al*. 2002). Spatial gradients of the sea level are dominated by the along-channel (2nd mode, 1.0%) and cross-channel (3rd mode, 0.2%) variations. The 4th mode (0.03%) reveals high levels in the central part of the Gulf and low levels near the coast, or vice versa, depending on the sign of the amplitude. This mode therefore represents amplification or decay of the mean cyclonic circulation.

Sea level gradients have significant dependence on wind direction. Along-channel gradients (2nd mode) are amplified by wind stress projected to 275° (R^2 = 0.77) and cross-channel gradients (3rd mode) by wind stress projected to 195° (R^2 = 0.49). In other words, sea level rises in the eastern end of the Gulf by the westerly wind stress component and on the northern shore by the southerly (slightly south-westerly) wind stress component. The 4th mode of the sea level gradients is excited by the westerly wind stress component (direction 285°, R^2 = 0.39) and the amplitudes correlate with the 3rd "circulation" mode of the surface currents (R^2 = 0.55).

The currents below the surface Ekman layer are forced by the sea level gradients and dynamically adjusted baroclinic pressure gradients. In order to suppress the possible distortions from the highly dominating almost uniform first sea level mode, the sea level gradients were decomposed into EOF modes separately. The along- and cross-channel gradient modes yield 23% and 17% of the total gradient variance, respectively. The amplitude correlation with the original sea level is high (R^2 = 0.92) for the cross-channel components and lower (R^2 = 0.73) for the along-channel components. On both analyzed current depth levels, 24–30 m (thermocline) and 50–60 m (halocline), the two first dominating current modes are quite homogeneous. The flow components are oriented along the main axis of the Gulf (24% of variance in the thermocline and 40% in the halocline) and along the transverse cross-channel direction (13% and 16%, respectively). The along-channel flow (1st current mode) is related to the cross-channel sea level gradients (2nd mode) in the thermocline with R^2 = 0.71 and in the halocline R^2 = 0.46. The transverse flow (2nd current mode) is correlated with the along-channel sea level gradients (1st mode), a bit more (R^2 = 0.64) in the halocline than in the thermocline (R^2 = 0.50). Therefore, we conclude that an evident geostrophic relation exists between the dominating sea level gradients and the flows below the surface Ekman layer.

In the frequency domain, the amplitudes of the wind modes have dominating energy in the synoptic range with a peak from 80 to 110 h. Most energetic, 1st sea level mode exhibits spectral maximum on the period of 31 h. Higher sea level modes are dominated by 24 h oscillations. We note that energetic diurnal tidal oscillations have been found also by the spectral analysis of observational data at selected sites in the Gulf of Finland (Johansson *et al*. 2001). Currents on the fixed levels are dominated either by the 24 h oscillations (1st mode) or inertial oscillations (higher modes). However, the 2nd ("cross-channel") and 3rd ("circulation") modes have maxima also in the low-frequency range, on the periods about 66 h and 30 days, respectively. During the strong upwelling event on the southern (Estonian) coast in July–August 2006 (Lips *et al*. 2008a), the amplitude of the 3rd surface current mode revealed distinct anomaly throughout the whole period.

Section modes

Further we studied the details of circulation patterns on selected meridional (cross-channel) sections. Since the horizontal analysis of the wind fields, presented above, showed quasi-uniform patterns, then (not surprisingly) correlations of the wind amplitudes between individual sections yield R^2 above 0.9. The same is valid for the 1st mode of the sea level variations.

First four modes of the east-west current anomalies cover 74% of the variance in section B (Fig. 6). In other sections of the western and central areas (A and C), both the geometry of patterns and the fractions of explained variance are similar. The amplitudes of the current modes are well correlated ($R^2 > 0.8$).in the western part between A and B, and less correlated ($0.4 < R^2 < 0.6$) in the eastern part of the central area between B and C. Further to the east, in the wider area of the Gulf (sections D and E) the similarity of the mode geometry and the correlations are lost.

The modes of density anomalies in the section B are depicted in Fig. 7. Three first modes cover 88% of the variance. In different sections, the most energetic 1st mode (52%–55%) presents mainly the seasonal density variations (Haapala and Alenius 1994) — strengthening of stratification during summer and weakening during winter — and is therefore highly coherent between all the different sections. Higher density

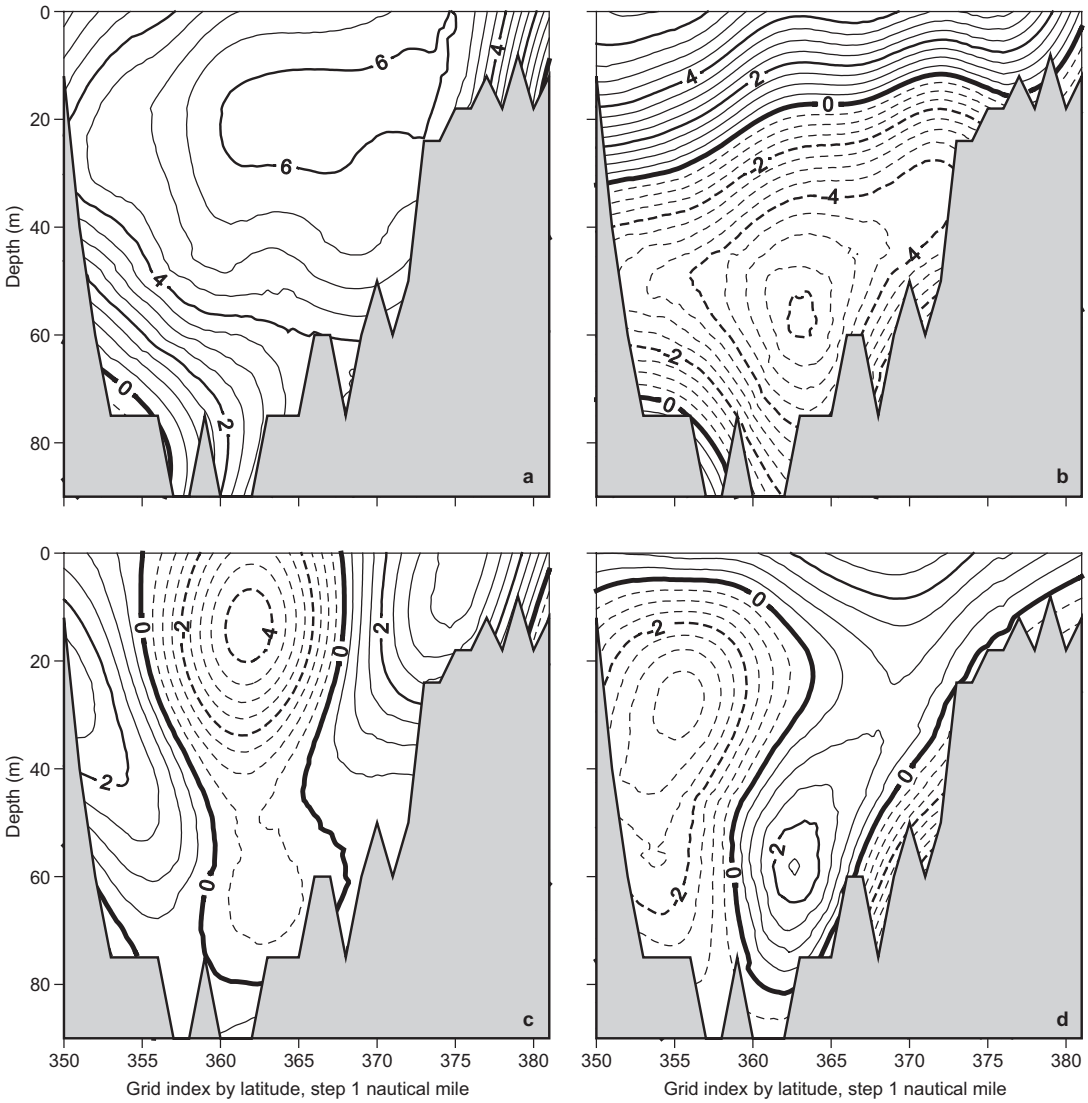

Fig. 6. Patterns of EOF modes of the east-west currents in the section B: (**a**) current U mode 1 (42%), (**b**) current U mode 2 (18%), (**c**) current U mode 3 (7%), and (**d**) current U mode 4 (6%). The mode patterns are dimensional (cm s^{-1}), scaled by the square root of the variance of each mode.

modes describe stratification disturbances due to the circulation variability. The geometrical similarity of these modes is apparent only from section A to C. Change of mean over section density is governed by the 2nd almost flat mode (22%–27%).

EOF analysis gives some physically meaningful modes. The 1st current EOF (23%–42%) is a flat ("barotropic") mode, characterized by unidirectional flow through the whole section. By amplitude variability it is related to the short-term (hours to days, spectral peak at 24 h) water storage variations in the Gulf, since correlation with the time derivative of the sea level 1st mode amplitude is acceptable ($R^2 \approx 0.4$).

The 2nd current EOF (19%–22%) is an "Ekman" mode (surface Ekman transport with deeper compensation flow). The flows are opposite in the surface and deeper layers but unidirectional within a layer. In the frequency space the amplitudes are dominated by the inertial (14 h) and low-frequency (days to a few tens of days)

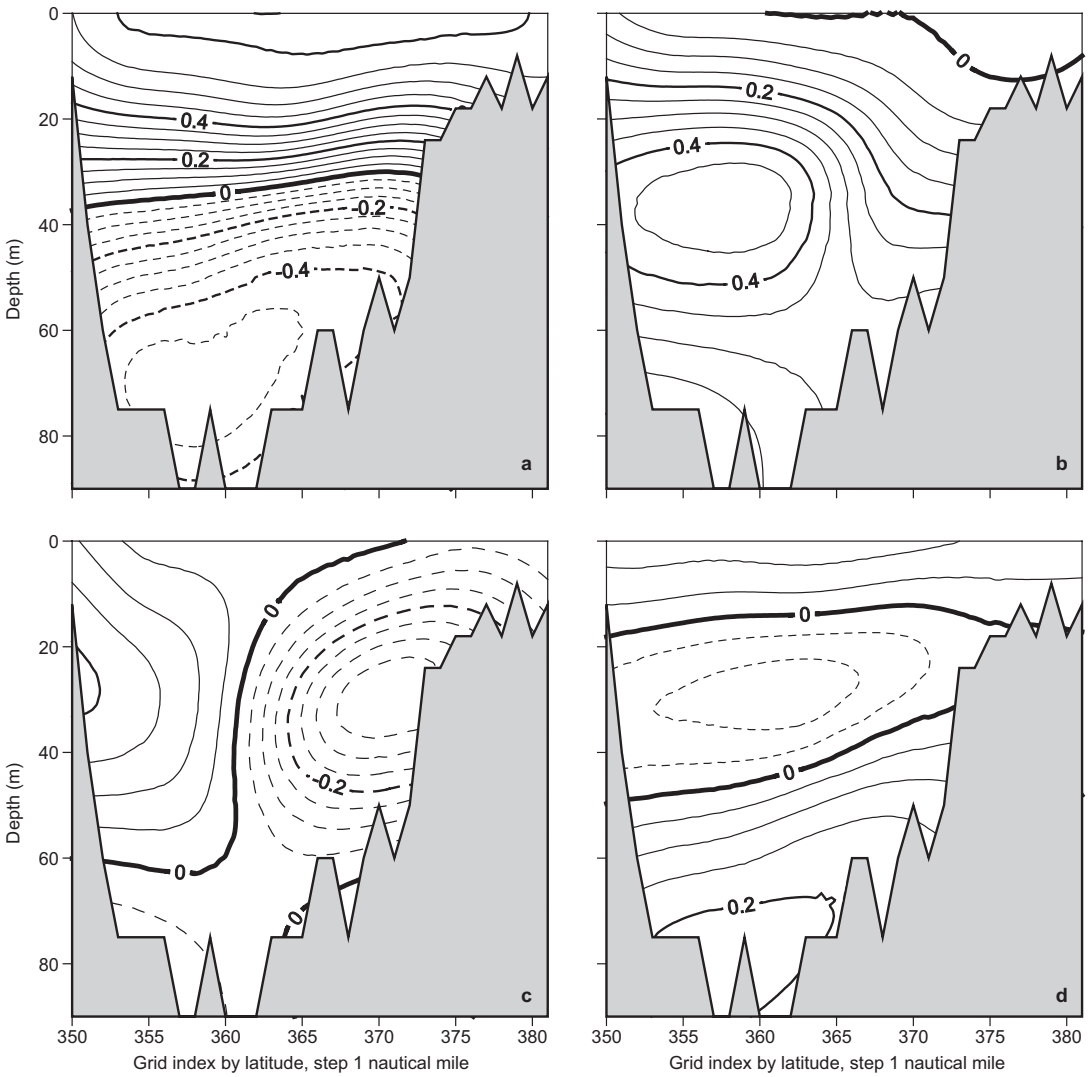

Fig. 7. Patterns of EOF modes of density in section B: (**a**) density mode 1 (55%), (**b**) density mode 2 (22%), (**c**) density mode 3 (10%), and (**d**) density mode 4 (4%). The mode patterns are dimensional (kg m^{-3}), scaled by the square root of the variance of each mode.

oscillations. By correlation analysis with the wind stress, highest surface layer outflow and deeper water inflow occur during north-easterly winds ($R^2 \approx 0.6$). Elken *et al*. (2003) obtained the same angle of wind stress projection, which provided the best correlation with the deep water outflow. We also made EOF detection of the joint east–west and north–south vector components. The joint 1st mode (32%) is "barotropic" for both of the current components. By the amplitudes, it is highly correlated ($R^2 > 0.9$) with the east–west component. The joint 2nd mode (15% of the variance) has similar geometry for the east–west component as the one-component mode (Fig. 6) and is well correlated with the latter ($R^2 \approx 0.8$). The north–south component of the joint mode has quite similar pattern geometry as the east-west component. It means that cross-channel flow components cause dynamical tilting of isopycnals.

The 3rd density EOF (15%–20%) is a thermocline "upwelling" mode that presents opposite density anomalies near the northern and southern coasts, concentrated in the mean (over

the seasons and years) pycnocline (≈ thermocline), located at depths of 35–40 m. The amplitudes of this mode did not show any correlations with wind stress projections. However, this density mode is acceptably ($R^2 \approx 0.4$) correlated with the 2nd "Ekman" mode of currents, which is furthermore correlated with the north-easterly wind stress projection. Unfortunately, analysis of the reasons for such a loss (or in some instances, gain) during correlation transfer is out of the scope of the present study.

The 3rd current EOF (6%–9%) presents a quite interesting structure of the "Bennett-Csanady" mode. In the long channels closed at least at one end, the steady flow is characterized by along-wind coastal jets and a compensation flow in the middle (deep part) of the channel with its maximum below the surface, since there is a competition between along-wind drift component and the return flow forced by the sea-level gradients established in a channel (Bennett 1974, Krauss and Brügge 1991). One might expect that this mode is amplified during the periods of persistent along-channel winds. We check this in the next sub-chapter.

Examples from EOF amplitude time series

Although the amplitudes of individual modes of the same data sets are uncorrelated over the whole period of determination, during specific events a joint excitement of different modes may occur.

One example of the amplitude time series behavior is given by a snapshot from July to September 2006 (Fig. 8), that covers the period of intense upwelling, observed near the southern coast of the Gulf from the end of July to the middle of August (Lips *et al*. 2009). Using the shipboard CTD measurements, the "normal" situation observed on 25 July was replaced on 8 August by upward displacement of the boundary of the upper mixed layer near the southern coast. The isotherm 10 °C was during the first survey everywhere at 10–20 m depths, but lifted by the second survey to the surface and shifted from the southern coast some 15–20 km offshore. The isohaline 6 psu, located during the first section at 10–30 m depths, also surfaced and shifted offshore by the same distance. Minimum surface salinities, that should be present in the water masses of the Finnish Coastal Current, were found on 8 August in the central part of the cross-gulf section. On 15–16 August and 22 August, further sections revealed relaxation of the upwelling process, i.e. warming of colder waters transported formerly to the surface from the deeper layers. The whole upwelling event was accompanied by the increase of salinity of deep layers.

The upwelling was created by the dominating easterly winds (Fig. 8a) that occurred from 29 July to 29 August. Sea level in Tallinn (both observed and modeled, Fig. 8b) was below the long-term average throughout the whole period. Standard deviations of model errors in respect to the sea level observations were 3.5 cm. Within this period, the model produced smaller amplitudes of the 25–28 h period seiches than observed. We can present the modeled sea levels in Tallinn (Fig. 8b) by the horizontal EOF modes, multiplying the sea level mode values in this location (Fig. 5) to the time series values of the amplitudes (Fig. 8d). The 1st flat mode gave maximum error 10 cm, but counting all the first 4 modes the maximum error reduced to 4 cm (Fig. 8c). Larger errors occurred on 15 August after sudden wind change from easterly to southerly and westerly directions. Such rapid wind changes occurred also later on 29 August and on 4 September. The amplitude of the 1st horizontal sea level mode (Fig. 8d) showed a negative value, corresponding to the lower than average sea level in the Gulf. The 2nd sea level mode (*see* the pattern in Fig. 5) was of positive amplitude (i.e. the sea level was lower in the eastern part of the Gulf than in the western part) and the 3rd mode was of negative amplitude (higher sea levels occurred near the northern coast due to the Ekman transport of easterly winds). Stronger easterly wind pulses took place from 29 July to 3 August and from 12 to 15 August. An interesting sea level feature is the amplification of the 4th horizontal "circulation" mode after 3 August. The amplitude value –3 (scaled to the standard deviation) corresponds to the cyclonic sea level doming with elevation about 3 cm in the central part of the Gulf.

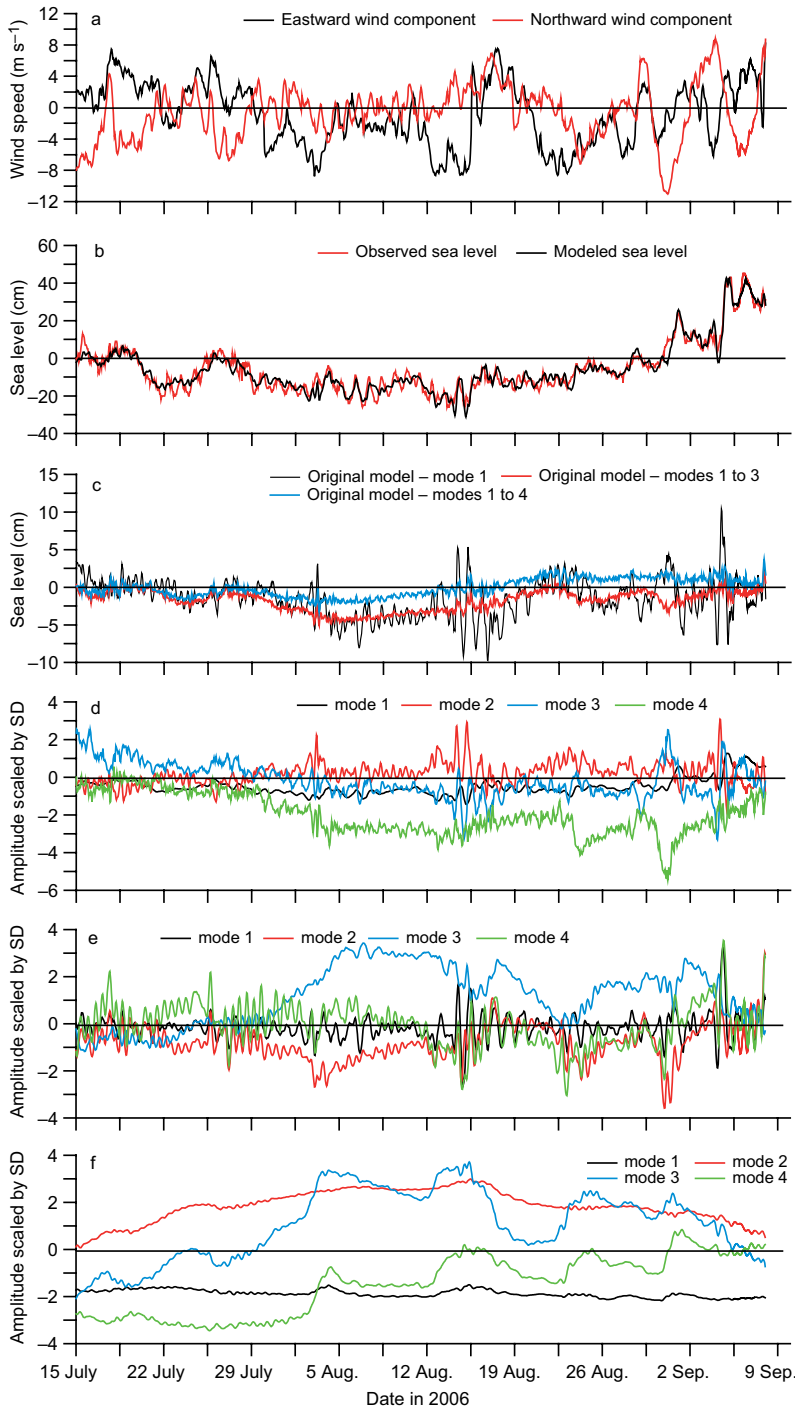

Fig. 8. Time series snapshot in July–September 2006: (**a**) wind components in the central gulf derived from the model forcing data; (**b**) observed and modeled sea level in Tallinn (*see* Fig. 1); (**c**) errors of sea level presentation in Tallinn by horizontal EOF modes (*see* Fig. 5) compared with the original modeled data, mode 1 and cumulatively the modes 1 to 3 and 1 to 4; (**d**) amplitudes of the first four EOF horizontal modes of sea level (*see* Fig. 5); (**e**) amplitudes of the first four EOF section modes of the east-west currents in section B (*see* Fig. 6); (**f**) amplitudes of the first four EOF section modes of density in section B (*see* Fig. 7). The EOF amplitudes (**d**–**f**) are non-dimensional, scaled by the condition that the standard deviation of each amplitude over the period of 2006–2008 is equal to 1.

The patterns of currents revealed 24 h to 30 h period oscillations of the amplitude (Fig. 8e) of the 1st barotropic mode around the value –0.28, that gives the mean westward speed up to 1.8 cm s^{-1}. The 2nd "Ekman" mode had an amplitude of –1.3 from 29 July to 15 August. This corresponds to the maximum of 12 cm s^{-1} westward flow in the surface layer (as can be

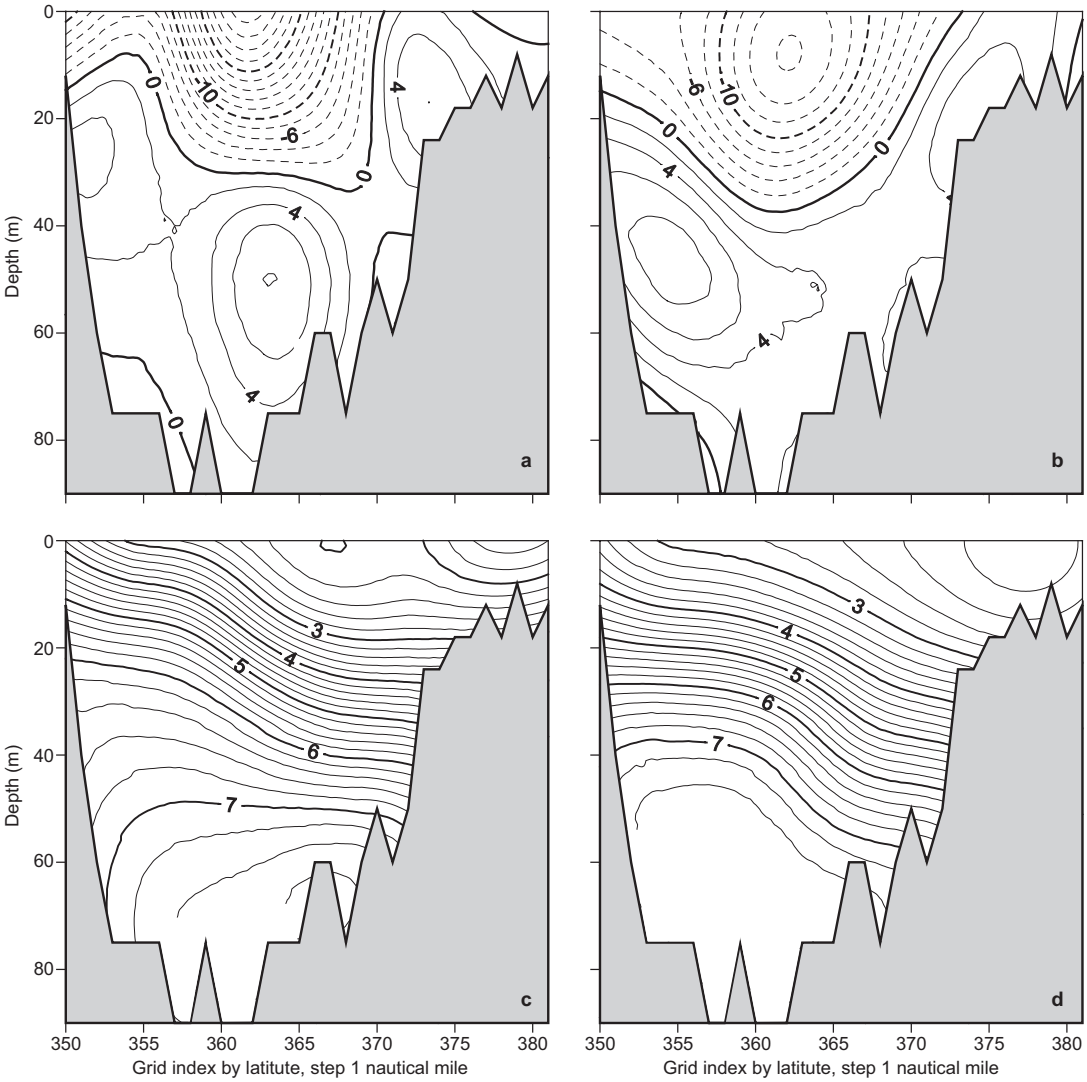

Fig. 9. Mean east–west currents (**a**, **b**) and density (**c**, **d**) in section B of period 9–12 August 2006, calculated from the model data (**a**, **c**) and as a sum of the four first EOF modes with the mean amplitudes over the period.

expected from the wind direction) and up to 8 cm s^{-1} eastward flow in deeper layers. The highest amplitude value — up to 3.4 standard deviations — had the 3rd ("Bennett-Csanady") section mode of currents (*see* the pattern in Fig. 6), that was persistent throughout the whole upwelling period. However, since the mode amplitude was positive, its presence has no direct physical explanation because the flow component due to this mode was against the wind direction in the more shallow coastal zones. By looking at the mean flow during the shorter period from 9 to 12 July (Fig. 9a, the mean wind was 3.9 m s^{-1} from 92°), the Finnish Coastal Current had shifted to the central axis of the Gulf. This feature is quite well reproduced by the superposition of the four first EOF modes, plus the mean flow over the longer period (Fig. 9b). Therefore the high amplitude of the 3rd mode was just a mathematical result of the EOF analysis to shift the Finnish Coastal Current southwards.

Amplitudes of density modes (Fig. 8f) revealed ordinary stronger summer stratification (negative amplitudes of the 1st mode, *see*

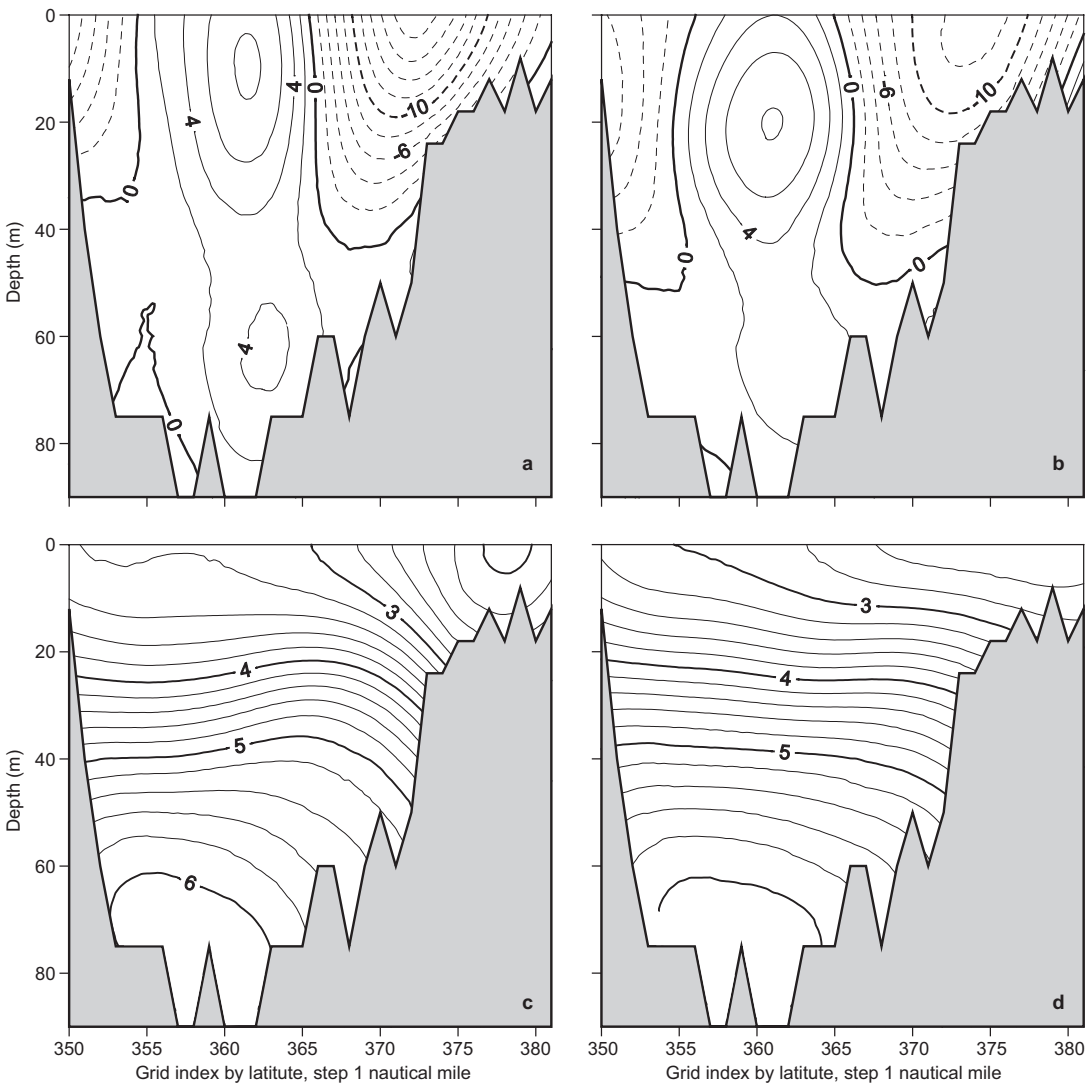

Fig. 10. Same as Fig. 9, but for the period 9–12 August 2007.

the pattern in Fig. 7), higher than usual mean density over the whole water column (positive amplitudes of the 2nd mode), and increase of density in the thermocline of the southern coast and its reduction near the northern coast (positive amplitudes of the 3rd mode from 29 July to 15 August). The amplitude time series of the 3rd "upwelling" density mode reflects the behavior of the 2nd "Ekman" mode of currents. Let us remind, that during the longer period the correlation of these modes was $R^2 = 0.4$. The modeled short-period mean density (Fig. 9d) with sloping isopycnals is close to the observed stratification during the upwelling (Lips *et al*. 2009). Again, as for the currents, the main characteristics of the density distribution are reproduced by the superposition of the four first EOF modes (Fig. 9d).

To compare the upwelling event in August 2006 with other periods of persistent winds, we present the mean currents and density in section B for the same dates as in 2006, but in 2007 (i.e. from 9 to 12 August 2007, Fig. 10). The mean wind in the central gulf was also 3.9 m s^{-1} but from 121°, still with easterly component as for 2006. The shorter period mean current (Fig. 10a) reveals the Finnish Coastal Current near

its long-term location on the northern slope of the Gulf. The mean amplitudes of the 1st and 2nd current modes were about 3 times smaller than in 2006. Among the EOF amplitudes during the period, the highest share — 1.9 times the standard deviation — had the amplitude of the 3rd "Bennett-Csanady" mode, whose sign was consistent with the channel flow theory. The resulting flow field, both in original model data and in superposition of the first four EOF modes (Fig. 10b), shows upwind compensation flow in the deeper part of the section. Mean flow is geostrophically consistent with the tilting of modeled isopycnals (Fig. 10c). Although the mean slopes are reproduced by the EOF modes well (Fig. 10d), the counter-flow in the deeper area is not in agreement with the monotonic tilting of EOF-derived isopycnals. The stratification in 2007 was considerably weaker than in 2006. Despite the similar short-term wind forcing during both years, the distributions of currents and density were quite different due to the different history of forcing.

Conclusions

Variance of the studied circulation and forcing fields, explained by the four first EOF modes, is high for the wind (96%) and sea level (99%). Horizontal modes of currents explain 71% of the variance on the surface and 67% in the halocline. On the meridional (about cross-gulf) sections of the western and central parts of the Gulf, three first density modes cover 86%–89% of the variance. Since the 1st density mode includes regular seasonal variations of the stratification, the explained "circulation" variability part of the leading density modes is lower than the above numbers. Indeed, the four first modes of east-west currents explained only 65%–73% of the variance. This moderate explanation rate (about 2/3) is not surprising, since the Gulf of Finland has intensive mesoscale and small-scale processes like eddies, frontal meanders, filaments, inertial waves etc., which cannot be presented by the basin scale coherent patterns.

Time series of EOF mode amplitudes contain interesting information. In several cases they allow quantitative estimation of qualitatively known cause-effect relationships within the complex ocean dynamics. Furthermore, the amplitude time series reflect well the main events in the basin scale circulation. Since EOF method is based on the products from the correlation matrix, we expect that extensions of EOF analysis, both by regions and studied variables, may contribute to the better assimilation schemes implemented in the operational models.

By the analysis of non-steady circulation patterns of the Gulf of Finland, we can distinguish two regions with a specific regime of variability.

Firstly, a western (near-mouth) wide channel that connects the entrance area to the central part of the Gulf. The topography is characterized by quasi-uniform width and cross-section area. Time-dependent wind forcing (the wind fields are quite homogeneous over the whole gulf, the flat modes cover 93% of the variance) creates similar along-channel current patterns on the cross-sections of the channel, as shown by the EOF modes. Time-dependent EOF amplitudes of the dominant modes correlate well between the sections.

Secondly, the eastern (near-head) wide basin that extends from the central part to the narrow estuary head. The flow dynamics here is more complex due to the topographical features and the vicinity of large freshwater source. We were not able to discover simple meridional patterns of circulation variability in this region, except for the patterns that are quasi-uniform over the whole gulf.

In the western, wide channel region, the dominating current variation (23%–42%) is barotropic (unidirectional flow over the whole section) oscillation (spectral peak at 24 h), that is related to the water storage variation of the Gulf. Two-layer flow (surface Ekman transport with deeper compensation flow, 19%–22%) has both the inertial and lower frequencies. In respect to the wind forcing, highest outflow of surface waters occurs during north-easterly winds. Third by energy (6%–9%) current pattern presents a quite interesting structure of the "Bennett-Csanady" mode: coastal jets and a compensation flow in the middle (deep part) of the channel, with a maximum below the surface. This mode in actual conditions usually appears in combination with other modes.

On the sea surface, quasi-uniform drift currents are deflected on the average by 40° to the right from the wind direction and they cover 60% of the circulation variance. Sea level variability is heavily (98%) dominated by almost uniform changes due to the water storage variations of the Gulf. Dominating sea level gradients are described by the main axis (23%) and the transverse (17%) components, forced by the winds of the same direction. Namely, the sea level rises in the eastern part of the Gulf during westerly winds and near the northern coast during southerly winds. The flows below the surface are also decomposed into the main axis (24%–40%) and the transverse (13%–16%) components, which are correlated with the sea level gradients according to the geostrophic relations.

Acknowledgements: The model data were kindly provided by the Swedish Meteorological and Hydrological Institute under the cooperation within BOOS (Baltic Operational Oceanographic System) and HIROMB (High Resolution Operational Model of the Baltic Sea). Friendly contribution by Lars Axell is highly appreciated. The analysis part of the study was supported by the grant no. 7328 of the Estonian Science Foundation.

References

Alenius P., Myrberg K. & Nekrasov A. 1998. The physical oceanography of the Gulf of Finland: a review. *Boreal Env. Res*. 3: 97–125.

Andrejev O., Myrberg K., Alenius P. & Lundberg P.A. 2004. Mean circulation and water exchange in the Gulf of Finland — a study based on three-dimensional modelling. *Boreal Env. Res*. 9: 1–16.

Axell L. 2006. *Weaker surface currents in HIROMB 3.1*. 9th HIROMB Scientific Workshop 28–31 August 2006, SMHI, Gothenburg, available at http://www.environment.fi/download.asp?contentid=56290&lan=en.

Bennett J.R. 1974. On the dynamics of wind-driven lake currents. *J. Phys. Oceanogr.* 4: 400–414.

Bergström S. & Carlsson B. 1994. River runoff to the Baltic Sea. *Ambio* 23: 280–287.

Chant R.J., Geyer W.R., Houghton R., Hunter E. & Lerczak J. 2007. Estuarine boundary layer mixing processes: insights from dye experiments. *J. Phys. Oceanogr.* 37: 1859–1877.

Elken J., Raudsepp U. & Lips U. 2003. On the estuarine transport reversal in deep layers of the Gulf of Finland. *J. Sea Res*. 49: 267–274.

Elken J., Kõuts T., Lagemaa P., Lips U., Raudsepp U. & Väli G. 2008. Sub-regional observing and forecast system for the NE Baltic: needs and first results. In: *US/EU Baltic Symposium "Ocean Observations, Ecosystem-Based Management & Forecasting", Tallinn, 27–29 May, 2008*, IEEE Conference Proceedings, doi:10.1109/BALTIC.2008.4625551.

Funkquist L. 2001. HIROMB, an operational eddy-resolving model for the Baltic Sea. *Bulletin of the Maritime Institute in Gdansk* 28: 7–16.

Gästgifvars M., Lauri H., Sarkanen A., Myrberg K., Andrejev O. & Ambjörn C. 2006. Modelling surface drifting of buoys during a rapidly-moving weather front in the Gulf of Finland, Baltic Sea. *Estuarine, Coastal and Shelf Science* 70: 567–576.

Gästgifvars M., Müller-Navarra S., Funkquist L. & Huess V. 2008. Performance of operational systems with respect to water level forecasts in the Gulf of Finland. *Ocean Dynamics* 58: 139–153

Gill A. 1982. *Atmosphere–ocean dynamics*. Academic Press.

Haapala J. & Alenius P. 1994. Temperature and salinity statistics for the Northern Baltic Sea 1961–1990. *Finnish Mar. Res*. 262: 51–121.

Johansson M., Boman H., Kahma K.K. & Launiainen J. 2001. Trends in sea level variability in the Baltic Sea. *Boreal Env. Res*. 6: 159–179.

Jönsson B., Döös K., Nycander J. & Lundberg P. 2008. Standing waves in the Gulf of Finland and their relationship to the basin-wide Baltic seiches. *J. Geophys. Res*. 113: C03004, doi:10.1029/2006JC003862

Krauss W. & Brügge B. 1991. Wind-produced water exchange between the deep basins of the Baltic Sea. *J. Phys. Oceanogr.* 21: 373–384.

Lass H.U. & Talpsepp L. 1993. Observations of coastal jets in the Southern Baltic. *Cont. Shelf Res*. 13: 2–3: 189–203.

Lehmann A. & Hinrichsen H.H. 2001. The importance of water storage variations for water balance studies of the Baltic Sea. *Phys. Chem. Earth B* 26: 383–389.

Lehmann A., Krauss W. & Hinrichsen H.H. 2002. Effects of remote and local atmospheric forcing on circulation and upwelling in the Baltic Sea. *Tellus* 54A: 299–316.

Lehmann A. & Myrberg K. 2008. Upwelling in the Baltic Sea — a review. *J. Mar. Systems* 74: S3–S12

Lips U., Lips I., Liblik T. & Elken J. 2008a. Estuarine transport *versus* vertical movement and mixing of water masses in the Gulf of Finland (Baltic Sea). In: *US/EU Baltic Symposium "Ocean Observations, Ecosystem-Based Management & Forecasting", Tallinn, 27–29 May, 2008*, IEEE Conference Proceedings, doi:10.1109/BALTIC.2008.4625535.

Lips U., Lips I., Kikas V. & Kuvaldina N. 2008b. Ferrybox measurements: a tool to study meso-scale processes in the Gulf of Finland (Baltic Sea). In: *US/EU Baltic Symposium "Ocean Observations, Ecosystem-Based Management & Forecasting", Tallinn, 27–29 May, 2008*, IEEE Conference Proceedings, doi:10.1109/BALTIC.2008.4625536.

Lips I., Lips U. & Liblik T. 2009. Consequences of coastal upwelling events on physical and chemical patterns in the central Gulf of Finland (Baltic Sea). *Cont. Shelf Res*. 29: 1836–1847.

Matthäus W. & Schinke H. 1999. The influence of river runoff on deep water conditions of the Baltic Sea. *Hyd-*

robiologia 393: 1–10.

Meier H.E.M. 2005. Modeling the age of Baltic Sea water masses: quantification and steady state sensitivity experiments. *J. Geophys. Res.* 110: C02006 doi: 101029/2004JC002607

Myrberg K., Ryabchenko V., Isaev A., Vankevich R., Andrejev O., Bendtsen J., Erichsen A., Funkquist L., Inkala A., Neelov I., Rasmus K., Rodriguez Medina M., Raudsepp U., Passenko J., Söderkvist J., Sokolov A., Kuosa H., Anderson T.R., Lehmann A. & Skogen M. D. 2010: Validation of three-dimensional hydrodynamic models of the Gulf of Finland. *Boreal Env. Res.* 15: 453–479.

Nerheim S. 2004. Shear-generating motions at various length scales and frequencies in the Baltic Sea — an attempt to narrow down the problem of horizontal dispersion. *Oceanologia* 46: 477–503.

Palmén E. 1930. Untersuchungen über die Strömungen in den Finnland umgebenden Meeren. *Soc. Sci. Fenn., Comm. Phys.-Math.* 12: 1–94.

Pizarro O. & Shaffer G. 1998. Wind-driven, coastal-trapped waves off the Island of Gotland, Baltic Sea. *J. Phys. Oceanogr.* 28: 2117–2129.

Reissmann J.H., Burchard H., Feistel R., Hagen E., Lass H.U., Mohrholtz V., Nausch G., Umlauf L. & Wieczorek G. 2009. Vertical mixing in the Baltic Sea and consequences for eutrophication — a review. *Progr. Oceanogr.* 82: 47–80.

Schrum C., St. John M. & Alekseeva I. 2006. ECOSMO, a coupled ecosystem model of the North Sea and Baltic Sea: Part II. Spatial-seasonal characteristics in the North Sea as revealed by EOF analysis. *J. Mar. Syst.* 61: 100–113.

Stipa T. 2004. Baroclinic adjustment in the Finnish coastal current. *Tellus* 56A: 79–87.

Thomson R.E., Mihály S.F. & Kulikov E.A. 2007. Estuarine *versus* transient flow regimes in Juan de Fuca Strait. *J. Geophys. Res.* 112: C09022, doi: 10.1029/2006JC003925.

Umlauf L., Burchard H. & Hutter K. 2003. Extending the κ-ω turbulence model towards oceanic applications. *Ocean Modelling* 5: 195–218.

von Storch H. & Zwiers F.W. 1999. *Statistical analysis in climate research*. Cambridge University Press, Cambridge.

Watterson I.G. 2001. Decomposition of global ocean currents using a simple iterative method. *J. Atmos. Oceanic Technol.* 18: 691–703.

Witting R. 1912. *Zusammenfassende Übersicht der Hydrographie des Bottnischen und Finnischen Meerbusens und der nördlichen Ostsee nach den Untersuchungen bis Ende 1910*. Finnländische hydrographisch-biologische Untersuchungen 7.